ISSN: 0067-2904

Matter Density Distributions and Reaction Cross Sections for ^{8}Li and ^{22}N Exotic Nuclei

Suhaib Q. Abdullah*, Ahmed N. Abdullah
Department of Physics, College of Science, University of Baghdad, Baghdad, Iraq

Received: 22/5/2021 Accepted: 17/8/2021

Abstract

The Harmonic Oscillator (HO) and Gaussian (GS) wave functions within the Binary Cluster Model (BCM) were employed to investigate neutron, proton and matter densities of the ground state as well as the elastic proton form factors of one neutron ^{8}Li and ^{22}N halo nuclei. The long tail is a property that is clearly shown in the neutron density. The existence of a long tail in the neutron densities of ^{8}Li and ^{22}N indicates that these nuclei have a neutron halo structure. Moreover, the matter rms radii and the reaction cross section (σ_R) of these nuclei were calculated using the Glauber model.

Keywords: Binary cluster model, neutron halo, Glauber model

توزيعات الكثافة المادية والمقاطع العرضية للتفاعل للنوى الغريبة ^{8}Li و ^{22}N

صهيب قصي عبدالله* وأحمد نجم عبدالله
قسم الفيزياء، كلية العلوم، جامعة بغداد، بغداد، العراق

الخلاصة:

تم استخدام الدوال الموجية لجهدي المتذبذب التوافقي و جاوس مع الأنموذج العنقودي الثنائي لدراسة توزيعات الكثافة النيوترونية، البروتونية والمادية للحالة الأرضية و عوامل التشكل المرنة لنوى الهالة الغنية بالنيوترونات ^{8}Li و ^{22}N. الامتداد الطويل ظهر بوضوح في توزيعات الكثافة النيوترونية لهذه النوى. انصاف الاقطار النووية المادية والمقاطع العرضية للتفاعل لهذه النوى تم دراستها باستخدام نموذج Glauber.

1. Introduction

The phenomena of nuclei far from β-stability are possible to be studied due to the experimental progress of radioactive ion beams. The neutron halos in some neutron-rich nuclei was an exciting discovery observed by interaction cross section measurements [1,2]. A series of nuclei near the neutron drip line were identified, in which neutron halo or neutron skin exists [3-5]. However, the behavior of the proton halo is different from that of the neutron halo because the repulsive Coulomb barrier is responsible for halo formation. The measurements of the reaction cross section (σ_R) have been used to estimate the sizes and matter distributions of exotic nuclei using the Optical Limit Approximation (OLA) of the Glauber model [6].

The valence neutron in the nucleus ^{8}Li has small separation energy of 2.032 MeV. This suggests that ^{8}Li is an interesting candidate for exploring the halo structure formation. Many calculations, such as the shell model, ab initio calculations, the cluster model, the relativistic

*Email: suhaibalhamad01@gmail.com

mean field and the Hartree-Fock method have been considered to study the halo nuclei structure [7-10]. Abdullah [11] used the Binary Cluster Model (BCM) and the Two-Frequency Shell Model (TFSM) to study the ground state matter densities of neutron-rich ^{6}He and ^{11}Li halo nuclei. Calculations showed that both models provide a good description on the matter density distribution of the above nuclei. The root-mean square (rms) proton, neutron and matter radii of these halo nuclei were successfully obtained by TFSM. The elastic charge form factors for these halo nuclei were studied through combining the charge density distribution obtained by TFSM with the Plane Wave Born Approximation (PWBA). Fan et al. [12] used the transmission method at intermediate energies to measure σ_R of ^{8}Li using ^{9}Be, ^{12}C, ^{27}Al, and proton targets. Using a modified Glauber model, they calculated the density distribution of ^{8}Li. Abdullah [13] has investigated the ground state features such as the proton, neutron and matter densities, the rms nuclear radii of unstable neutron-rich ^{14}B, ^{15}C, ^{19}C and ^{22}N nuclei using the cosh potential radial wave functions within the two-body model of (Core+*n*). The obtained results showed that the cosh potential radial wave functions of the two-body model are capable of reproducing neutron halo in these nuclei.

In this work, the harmonic oscillator (HO) and Gaussian (GS) wave functions within the BCM were employed to investigate neutron, proton and matter densities in the ground state as well as the elastic proton form factors of one neutron ^{8}Li and ^{22}N halo nuclei. Moreover, matter rms radii and the reaction cross section (σ_{R}) of these nuclei were calculated using the Optical Limit Approximation (OLA) of Glauber model.

2. Theory

The halo nuclei in BCM [14] are treated as composite projectiles (Figure 1) with an A_p mass as core and halo (valence) clusters with masses of A_c and A_v ,respectively, bounded with a state of relative motion. It is assumed that $A_c \geq A_v$. The matter density of the composite projectile is given by [15]:

$$\rho_m(r) = \rho_c(r) + \rho_v(r), \tag{1}$$

where the core and valence densities are denoted by $\rho_c(r)$ and $\rho_v(r)$, respectively.

Two distributions were adopted in this study, namely; harmonic oscillator (HO) and Gaussian (GS) distributions.

The densities of the core and halo clusters in the HO distribution are described using HO wave functions [16]:

$$\rho_c(r) = \frac{1}{4\pi}\sum_{n\ell} X_c^{n\ell} \left|R_{n\ell}(r, \hat{b}_c)\right|^2 \tag{2}$$

$$\rho_v(r) = \frac{1}{4\pi} X_v^{n\ell} \left|R_{n\ell}(r, \hat{b}_v)\right|^2 \tag{3}$$

where $X^{n\ell}$ represents the number of protons or neutrons and $R_{n\ell}(r)$ is the radial wave functions of HO potential.

Whereas, the densities of the core and halo clusters in the GS distribution are described using GS wave functions [14]:

$$\rho_m(r) = A_c\, g^{(3)}(\hat{\alpha}_c, r) + A_v\, g^{(3)}(\hat{\alpha}_v, r), \tag{4}$$

where $g^{(3)}$ is the Gaussian function.

$$g^{(3)}\left(\hat{\alpha}_{c(v)}, r\right) = \frac{1}{\pi^{3/2}\hat{\alpha}_{c(v)}^3}\, e^{-r^2/\hat{\alpha}_{c(v)}^2}, \qquad \int g^{(3)}\left(\alpha_{c(v)}, r\right) d\vec{r} = 1 \tag{5}$$

The GS $\left({\hat{\alpha}_c}^2,\ {\hat{\alpha}_v}^2\right)$ and HO $\left({\hat{b}_c}^2,\ {\hat{b}_v}^2\right)$ size parameters are given by [14,16]:

$${\hat{g}_c}^2 = {g_c}^2 + \left(\frac{A_v g}{A_v + A_c}\right)^2, \qquad {\hat{g}_v}^2 = {g_v}^2 + \left(\frac{A_c g}{A_v + A_c}\right)^2, \ g \equiv \alpha, b \tag{6}$$

The matter density distribution in Eq. (1) can be written in terms of neutron density $[\rho^n(r)]$ and proton density $[\rho^p(r)]$ as follows [17]:

$$\rho_m(r) = \rho^n(r) + \rho^p(r), \tag{7}$$

where

$$\rho^n(r) = \rho_c^n(r) + \rho_v^n(r) \tag{8}$$

and

$$\rho^p(r) = \rho_c^p(r) + \rho_v^p(r) \tag{9}$$

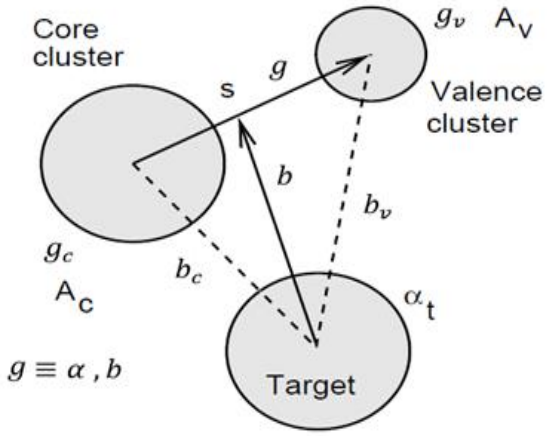

Figure 1- The coordinates of the target and two-cluster projectile [14].

The elastic form factors for the investigated nuclei are calculated using the proton densities obtained via HO distributions with the Plane Wave Born Approximation (PWBA), which can be represented as [18]:

$$F(q) = \frac{4\pi}{Z} \int_0^\infty \rho_p(r) j_0(qr) r^2 dr, \tag{10}$$

where $j_0(qr)$ is the zero-order spherical Bessel function and q is the momentum transfer from the incident electron to the target nucleus. Inclusion of the corrections of the finite nucleon size $F_{fs}(q) = exp(-0.43q^2/4)$ and the center of mass $F_{cm}(q) = exp(b^2q^2/4A)$ in the calculations needs multiplying the form factor of Eq. (10) by these corrections.

The GS wave functions within the OLA of the Glauber model is employed to calculate the σ_R of the considered nuclei which can be written as [19]:

$$\sigma_R = 2\pi \int [1 - T(b)]\, b\, db, \tag{11}$$

where $T(b)$ is the transparency function at impact parameter b.
The $T(b)$ in the OLA is given by [14]:

$$T(b) = \left|S_{el}^{OL}(b)\right|^2, \tag{12}$$

where $S_{el}^{OL}(b)$ is the elastic *S*-matrix for the target-projectile system given as [14]:

$$S_{el}^{OL}(b) = exp[iO_{PT}(b)] \tag{13}$$

The overlap $[O_{PT}(b)]$ of the projectile and target ground state densities ($\rho_P$and ρ_T, respectively) is given as [14]:

$$O_{PT}(b) = \int_{-\infty}^{\infty} dR_3 \int d\vec{r}_1 \int d\vec{r}_2 \rho_P(r_1)\rho_T(r_2) f_{NN}\left(\left|\vec{R} + \vec{r}_1 - \vec{r}_2\right|\right) \tag{14}$$

3. Results and discussion

The BCM with the HO and GS wave functions were used to study the neutron, proton and matter densities of the ground state as well as the elastic proton form factors of one neutron

^{8}Li (S_n=2.032 Mev, $\tau_{1/2}$ = 8.399 s) and ^{22}N (S_n= 1.28MeV $\tau_{1/2}$ = 24 ms) [20, 21] halo nuclei. Two distributions in BCM calculations were adopted which are: HO and GS distributions. Moreover, the matter rms radii and σ_R of selected nuclei were calculated using the OLA of Glauber model.

The HO wave functions were used to describe the densities of the core and halo clusters in the HO distribution. It was considered that ^{8}Li [^{22}N] is composed of one valence neutron in $1p_{1/2}$ [$2s_{1/2}$] with ^{7}Li [^{21}N] core nucleus which has the configuration $(1s_{1/2})^4$, $(1p_{3/2})^3$ [$(1s_{1/2})^4$, $(1p_{3/2})^8$, $(1p_{1/2})^3$, $(1d_{5/2})^6$]. The GS wave functions were used to describe the densities of the core and halo clusters in the GS distribution. The HO and GS size parameters used in the present calculations for selected halo nuclei were obtained by Eq. (6) and are tabulated in Table 1. The HO (b) and GS (α) size parameters for stable nuclei ^{6}Li and ^{15}N were adjusted to reproduce the experimental rms matter radii for these nuclei as shown in Table 2.

Table 1-The HO and GS size parameters for halo ^{8}Li and ^{22}N nuclei

Halo Nucleus	Core nucleus	HO		GS	
		$\hat{b}_c$ (fm)	$\hat{b}_v$ (fm)	$\hat{\alpha}_c$ (fm)	$\hat{\alpha}_v$ (fm)
^{8}Li	^{7}Li	1.589	3.288	1.604	3.821
^{22}N	^{21}N	1.820	3.959	2.135	5.229

Table 2- The HO and GS size parameters for stable ^{6}Li and ^{15}N nuclei

Stable nucleus	***b* (fm)**	**α (fm)**	**$\langle r_m^2 \rangle_{cal}^{1/2}$(fm)**		**$\langle r_m^2 \rangle_{exp}^{1/2}$ (fm) [22]**
			HO	GS	
^{6}Li	1.714	1.899	2.32	2.32	2.32±0.05
^{15}N	1.625	1.976	2.42	2.42	2.42±0.1

The calculated and experimental matter density distributions for ^{8}Li (parts *a* and *b*) and ^{22}N (parts *c* and *d*) halo nuclei are depicted in Figure 2 which are represented by dot-dash red curves and gray area [23, 24], respectively. The density distributions of the core and valence neutron are also plotted in this figure, the black and green curves. These distributions were calculated by the GS [Figures 2(a) and 2(c)] and HO [Figures 2(b) and 2(d)] methods. The significant property of the dot-dash red curves is the long tail (the distinctive property of halo nucleus). It was found from the above comparison between the calculated and the experimental results that the experimental matter density distributions for the selected halo nuclei are reproduced well by the present calculations using the GS and HO distributions.

In Figure 3 the black, green and dot-dash red curves represent the proton, neutron and matter density distributions, respectively. These distributions were calculated by the GS [Figures 3(a) and 3(c)] and HO [Figures 3(b) and 3(d)] methods. The long tail is a property that is clearly revealed in the density of the neutrons since it is found in halo orbits. Since protons are absent in the halo orbit and all protons of these nuclei are present in their cores, the black curves have a steep slope. The existence of a long tail in the neutron density distributions of ^{8}Li and ^{22}N indicates that these nuclei have a neutron halo structure.

In Figure 4, the dot-dash red and green curves represent matter densities of unstable (^{8}Li, ^{22}N) and stable (^{6}Li, ^{15}N) nuclei, respectively. The dot-dash red curves extend much farther than the green curves due to the weak binding of the last neutron in ^{8}Li and ^{22}N.

The proton densities obtained by HO distributions within the PWBA are employed to calculate the elastic form factors of the unstable (^{8}Li, ^{22}N) and stable (^{6}Li, ^{15}N) nuclei which are presented in Figure 5. In this figure, the red and green curves correspond to the calculated C0 form factors of unstable and stable nuclei, respectively, whereas, the filled circle curves represent the experimental data of the stable nuclei ^{6}Li [25] and ^{15}N [26]. According to these calculated results, one diffraction minimum appears in each of the red and green curves. The

red curve minimum location shifts to the right due to the difference in the center of mass correction.

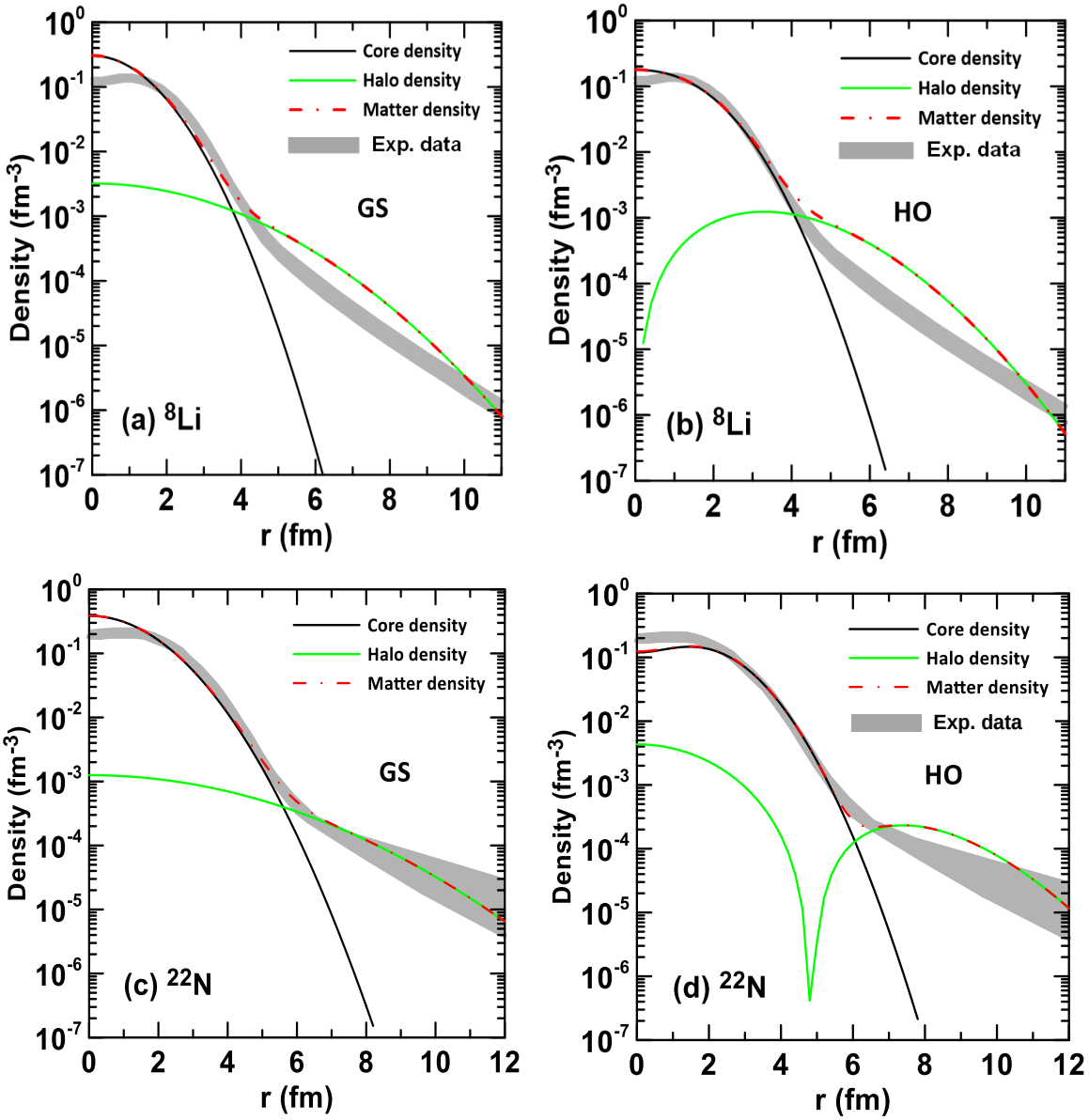

Figure 2-The calculated and experimental matter densities for halo ^{8}Li and ^{22}N nuclei.

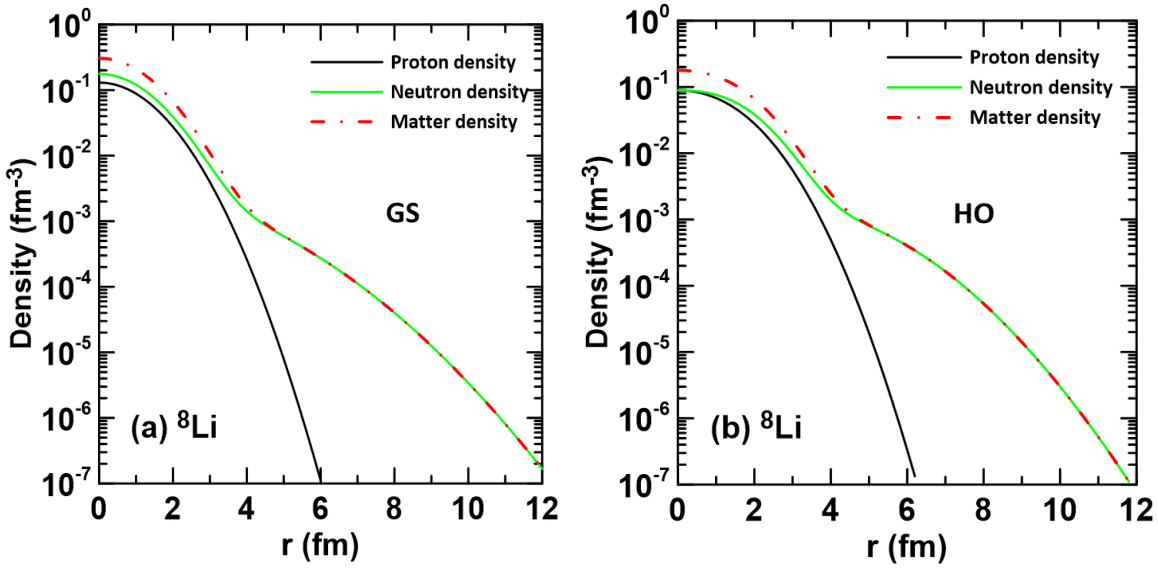

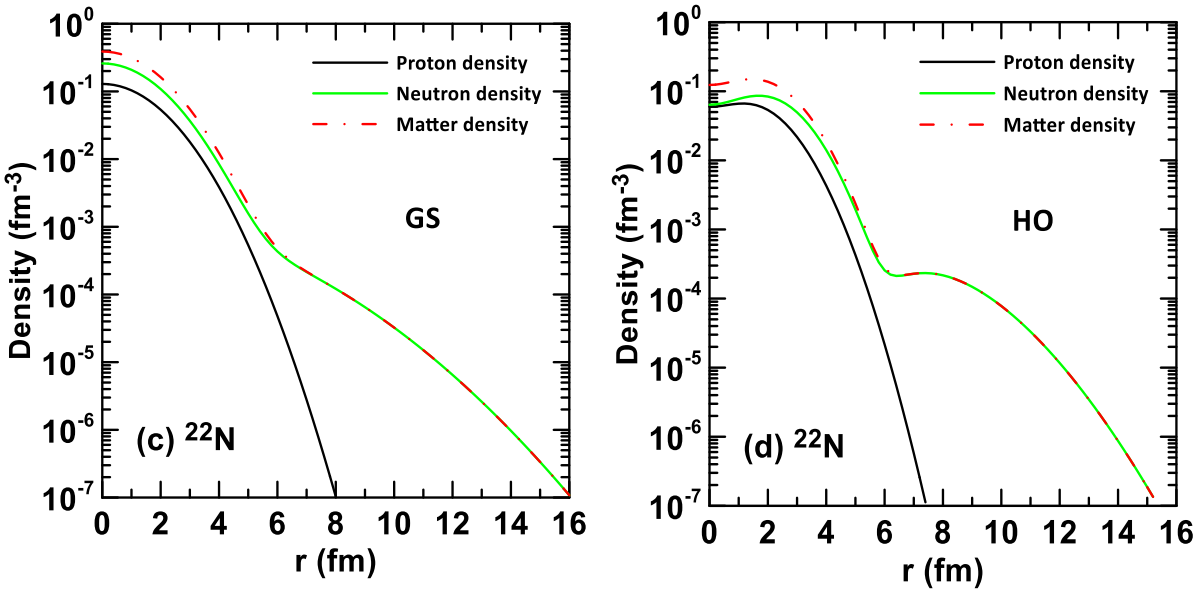

Figure 3-The proton, neutron and matter densities for halo ^{8}Li and ^{22}N nuclei.

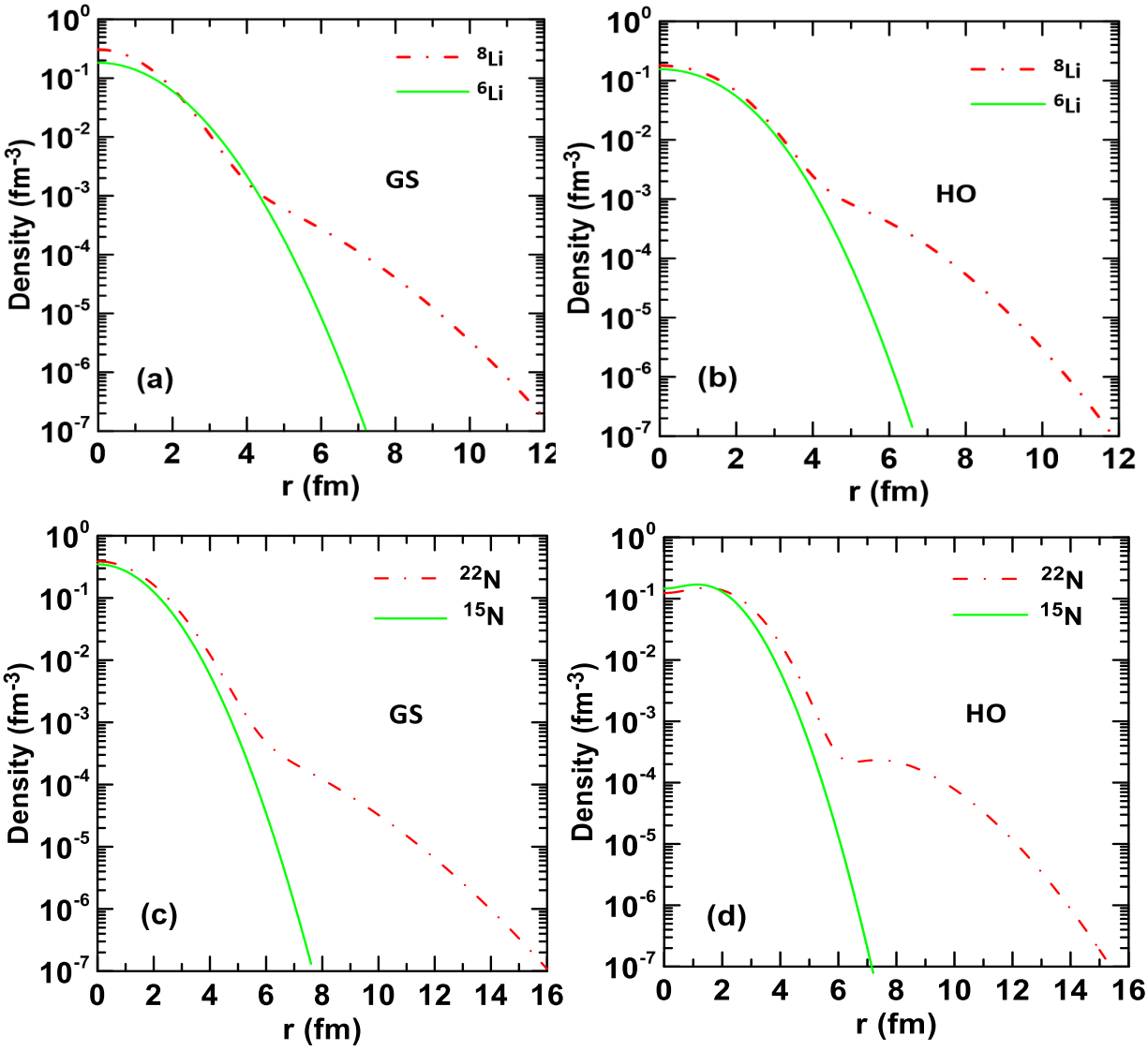

Figure 4-The calculated matter densities for ^{6,8}Li and ^{15,22}N nuclei.

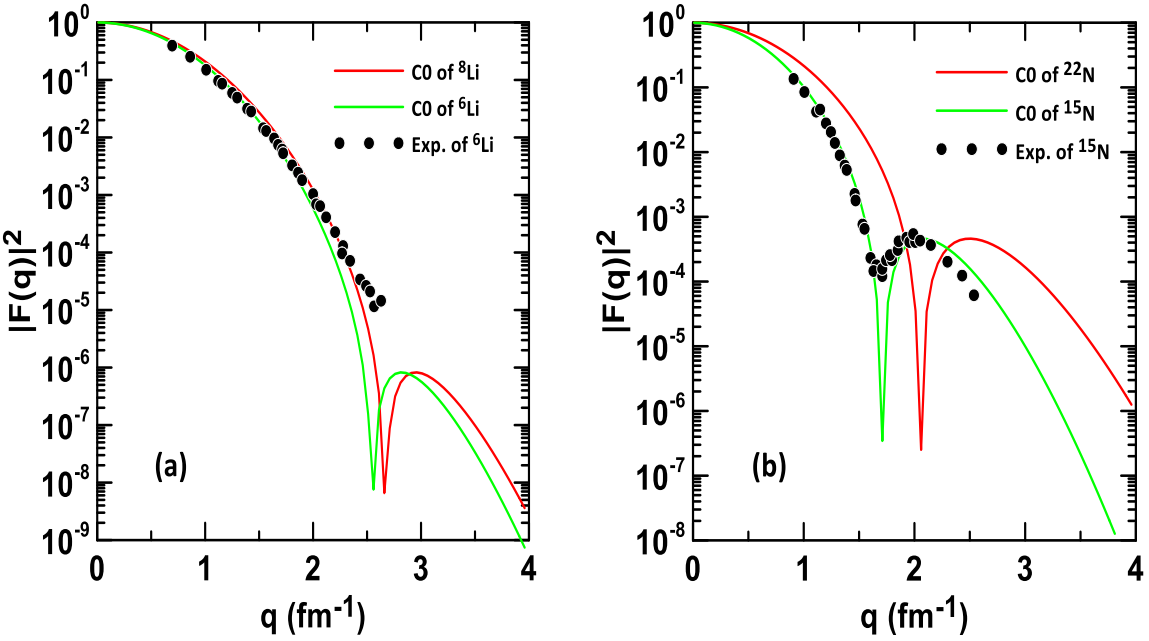

Figure 5- Elastic form factors for ^{6,8}Li and ^{15,22}N nuclei.

The GS wave functions within the OLA of the Glauber model were employed to calculate σ_R of ^{8}Li and ^{22}N nuclei on ^{12}C target. The obtained results are summarized in Table 3 together with the analogous experimental data [12, 27]. The calculated results give a good description of the experimental σ_R.

Table 3-The experimental and calculated σ_R for ^{8}Li and ^{22}N halo nuclei.

Halo nuclei	Energy (MeV) [12, 27]	Calculated σ_R (mb)	Experimental σ_R (mb) [12, 27]
^{8}Li	61	1044	1037 ± 17
	105	880	870 ± 13
	790	772	768 ± 9
^{22}N	965	1250	1245 ± 49

Figure 6 demonstrates the dependence of σ_R (in mb), calculated via the OLA of Glauber model, on matter rms radii (in fm) for ^{8}Li (Figure 6 (a)) and for ^{22}N (Figure 6 (b)) exotic nuclei on ^{12}C target at high energy. The green lines and the horizontal magenta lines are the calculated and the experimental σ_R, respectively, whereas the shaded area refers to the error bar of the experimental σ_R . The intersection point of the green line and magenta line refer to the calculated matter rms radius ($\langle r_m^2 \rangle^{1/2}$) of the halo nuclei. It is noted from Figure 6(a) for ^{8}Li [Figure 6(b) for ^{22}N] that the calculated $\langle r_m^2 \rangle^{1/2}$ of ^{8}Li [^{22}N] is equal to 2.495 [3.14] fm which give a good agreement with the experimental value 2.50±0.06 [3.08±0.13] fm [6, 27].

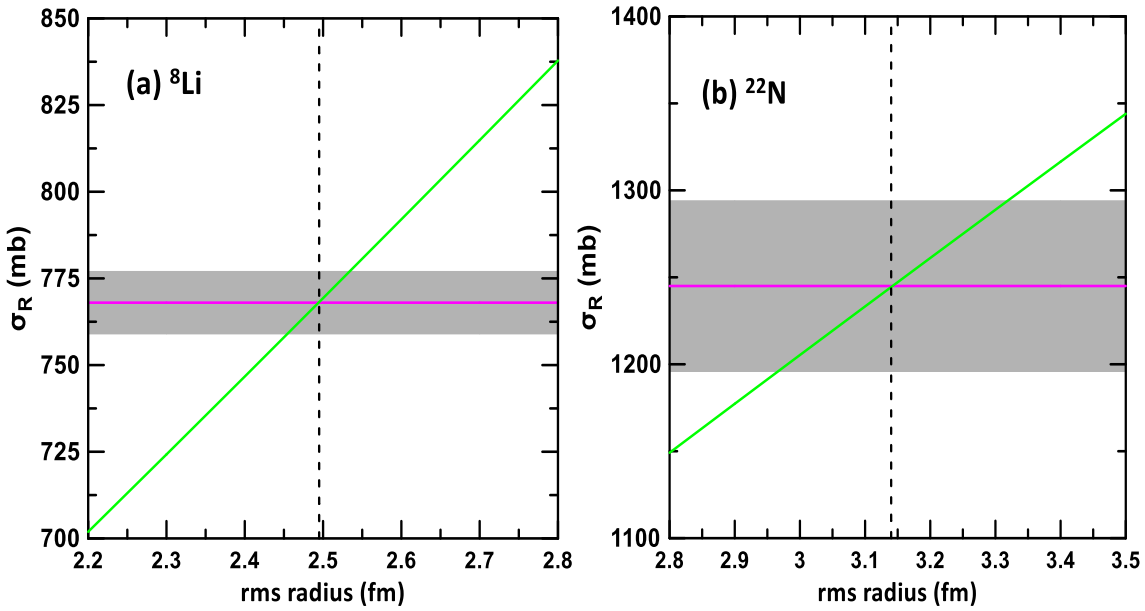

Figure 6- The dependence of the σ_R on the rms radii for halo ^{8}Li and ^{22}N nuclei.

4. Summary and conclusions

The HO and GS wave functions within the BCM were employed to investigate neutron, proton and matter densities in the ground state as well as the elastic proton form factors of one neutron ^{8}Li and ^{22}N halo nuclei. Two distributions in BCM calculations, namely: HO and GS distributions, were adopted. The experimental matter density distributions for selected halo nuclei were reproduced well by the present calculations using the GS and HO distributions. The long tail is a property that is clearly revealed in the density of the neutrons since it is found in halo orbits. The existence of a long tail in the neutron density distributions of ^{8}Li and ^{22}N indicates that these nuclei have a neutron halo structure. Moreover, the matter rms radii and σ_R of these nuclei were calculated using the OLA of Glauber model at high energy. The calculated results of matter rms radii and σ_R gave a good description of the experimental data.

Reference

[1] I. Tanihata, H. Hamagaki, O. Hashimoto, Y. Shida, N. Yoshikawa, K. Sugimoto, O. Yamakawa, T. Kobayashi, and N. Takahashi, Phys. Rev. Lett. 55, **1985**. 2676.

[2] I.Tanihata,H.Hamagaki,O.Hashimoto,S.Nagamiya,Y.Shida,N.Yoshikawa,O.Yamakawa,K.Sugimoto,T.Kobayashi,D.E.Greiner,N.Takahashi,Y.Nojiri, *Phys. Lett. B* 160(6), **1985**. 380.

[3] I. Tanihata, H. Savajols and R. Kanungo, *Prog. Part. Nucl. Phys.* **68, 2013**. 215.

[4] G. A. Korolev, A. V. Dobrovolsky, A. G. Inglessi, G. D. Alkhazov, P. Egelhof, A. Estradé, I. Dillmann, F. Farinon, H. Geissel, S. Ilieva, Y. Ke, A. V. Khanzadeev, O. A. Kiselev, J. Kurcewicz, X. C. Le, Yu. A. Litvinov, G. E. Petrov, A. Prochazka, C. Scheidenberger, L. O. Sergeev, H. Simon, M. Takechi, S. Tang, V. Volkov, A. A. Vorobyov, H. Weick and V. I. Yatsoura, *Phys. Lett. B* **780, 2018**. 200.

[5] A. V. Dobrovolsky, G. A. Korolev, A. G. Inglessi, G. D. Alkhazov, G. Colò, I. Dillmann, P. Egelhof, A .Estradé, F. Farinon, H. Geissel, S. Ilieva, Y. Ke, A. V. Khanzadeev, O. A. Kiselev, J. Kurcewicz, X. C. Le, Yu.A. Litvinov, G. E. Petrov, A. Prochazka, C. Scheidenberger, L. O. Sergeev, H. Simon, M. Takechi, S. Tang, V. Volkov, A. A. Vorobyov, H. Weick and V. I. Yatsoura, *Nucl. Phys. A* **989, 2019**. 40.

[6] A.V. Dobrovolsky, G.D. Alkhazov, M.N. Andronenko, A. Bauchet, P. Egelhof, S. Fritz, H. Geissel, C. Gross, A.V. Khanzadeev, G.A. Korolev, G. Kraus, A.A. Lobodenko, G. Münzenberg,

M. Mutterer, S.R. Neumaier, T. Schäfer, C. Scheidenberger, D.M. Seliverstov, N.A. Timofeev, A.A. Vorobyov and V.I. Yatsoura, Nucl. Phys. A **766**, **2006**. 1.

[7] H. Kitagawa and H. Sagawa, Phys. Lett. B **299**, 1, **1993**.

[8] Y. S. Shen and Z. Ren, Phys. Rev. C **54**, 1158, **1996**.

[9] M. Tomaselli, S. Fritzsche, A. Dax, P. Egelhof, C. Kozhuharov, T. Kühl, D. Marx, M. Mutterer, S.R. Neumaier, W. Nörtershäuser, H. Wang and H. J. Kluge, Nucl. Phys. A **690, 2001**. 298c.

[10] S. C. Pieper, K. Varga, and R. B. Wiringa, Phys. Rev. C **66**, **2002**. 044310.

[11] A. N. Abdullah, *Iraqi Journal of Science* **59** (2C), **2018**. 1057.

[12] G. W. Fan, M. Fukuda, D. Nishimura, X. L. Cai, S. Fukuda, I. Hachiuma, C. Ichikawa, T. Izumikawa, M. Kanazawa, A. Kitagawa, T. Kuboki, M. Lantz, M. Mihara, M. Nagashima, K. Namihira, Y. Ohkuma, T. Ohtsubo, Zhongzhou Ren, S. Sato, Z. Q. Shen, M. Sugiyama, S. Suzuki, T. Suzuki, M. Takechi, T. Yamaguchi, B. J. Xu and W. Xu, Phys. Rev. C **90**, **2014**. 044321.

[13] A. N. Abdullah, *Int. J. Mod. Phys. E* **29** (2020) 2050015.

[14] J. A. Tostevin, R. C. Johnson and J. S. Al-Khalili, *Nucl. Phys.* A **630**, **1998**. 340c.

[15] A. N. Abdullah, *Pramana – J. Phys.* **94**, **2020**. 154.

[16] A. K. Hamoudi and A. N. Abdullah, *Iraqi Journal of Science* **57**, **2016**. 2664.

[17] A. N. Abdullah, *Int. J. Mod. Phys. E* **26** (2017) 1750048.

[18] A. N. Antonov, M. K. Gaidarov, D. N. Kadrev, P. E. Hodgson and E. M. D. Guerra, *Int. J. Mod. Phys. E* **13**, **2004**. 759.

[19] F. D. Qing, M. C. Wang, M. Y. Gang, C. X. Zhou, C. J. Gen, C. J.Hui, G. Wei, T. W. Dong, W. Kun, W.Y. Bin, Y. T. Zhi, Z. Chen, Z. J. Xu and S. W. Qing, *Chin. Phys. Lett*. **22**, **2005**. 572.

[20] M. Wang, G. Audi, F.G. Kondev, W.J. Huang, S. Naimi and Xing Xu, Chin. Phys. C **41**, **2017**. 030003.

[21] G. Audi, F.G. Kondev, Meng Wang, W.J. Huang and S. Naimi, Chin. Phys. C **41**, 3, **2017**. 030001.

[22] S. Ahmad, A. A. Usmani, and Z. A. Khan, *Phys. Rev*. C **96**, **2017**. 064602.

[23] G. W. Fan, M. Fukuda, D. Nishimura, X. L. Cai, S. Fukuda, I. Hachiuma, C. Ichikawa, T. Izumikawa, M. Kanazawa, A. Kitagawa, T. Kuboki, M. Lantz, M. Mihara, M. Nagashima, K. Namihira, Y. Ohkuma, T. Ohtsubo, Zhongzhou Ren, S. Sato, Z. Q. Sheng, M. Sugiyama, S. Suzuki, T. Suzuki, M. Takechi, T. Yamaguchi and W. Xu, Phys. Rev. C **91**, **2015**. 014614.

[24] A. Ozawa Eur. Phys. J. A **13**, **2002**. 163.

[25] L. R. Suelzle, M. R. Qearian and H. C. Rannell, *Phys. Rev.* **162, 1967**. 992.

[26] E. B. Dally, M. G. Croissiaux and B. Schweitz, *Phys. Rev. C* **2**, **1970**. 2057.

[27] A. Ozawa, T. Suzuki and I. Tanihata, *Nucl. Phys*. A **693**, **2001**. 32.